UNIVERSITY OF JYVÄSKYLÄ

Evaluation of shot peening parameters with Barkhausen noise, residual stress and retained austenite content measurements

Jukka Wartiainen

Master's thesis
University of Jyväskylä
2018-12-31
Instructors: Markku Kataja (University of Jyväskylä)
Lasse Suominen (Stresstech Oy)

Foreword

This Master's Thesis for University of Jyväskylä (Department of Physics) has been carried out to examine a certain correlation between shot peening parameters, Barkhausen noise measurement, residual stress and retained austenite content results. Lasse Suominen (Stresstech Oy) and Dr. Markku Kataja (University of Jyväskylä) have been acting as the main instructors in this thesis project, with L. Suominen as the main instructor and Dr. M. Kataja regarding the writing process. During this thesis project, I've received a lot of help from many people including: Dr. Mikko Palosaari (Stresstech Oy), Henri Larjosuo (Stresstech Oy), J.P.O. Ahola (Stresstech Oy) and Dr. Suvi Santa-Aho (Techical University of Tampere). Without of them the project would probably would not have been finished. The project was carried out in Stresstech Oy's measurement service, which is managed by Dr. Mikko Palosaari.

I would like to thank all afore-mentioned people as well as my family for their everlasting support. In addition, I would like to thank Aki Sorsa (University of Oulu) for the final key in correlation calculations, Simon Francou (Scania AB) for great ideas and support during this thesis, and Anu Nuotto (Stresstech Oy) for clear and informational diagrams.

Abstract

This Master's thesis is concerned with answers to the correlation between shot peening parameters, Barkhausen noise and X-ray diffraction measurement results. The changes in residual stresses and hardness can be measured with Barkhausen noise method while X-ray diffraction method contributes exact result on a specific spot; shot peening is a post treatment method to increase fatigue and abrasion resistance in metallographic sample surfaces. The thesis has been commissioned by Stresstech Oy, and the studied samples were received from Scania AB. The Barkhausen noise measurements were carried out in the Technical University of Tampere, while X-ray diffraction measurements were carried out in Stresstech Oy.

During the thesis, multiple methods were tested to discover the correlation between the shot peening parameters, Barkhausen noise signal parameters, residual stress and retained austenite measurements. Only the most assuring results are presented in the thesis.

The amount of raw data is vast, therefore optimization was required. A polynomial of second degree was fitted into residual stress depth measurements up to 100 μm, polynomial constants *a, b* and *c*, function area and function derivative zero point were utilized in the correlation inspection. After several trials a multiple regression analysis was utilized, which produced the most promising results.

Based on the measurements, some remarkable correlations were found between the shot peening parameters, X-ray diffraction and Barkhausen noise measurements. Furthermore, the retained austenite content did not show much effect on correlation. The more important finding was that when the shot peening intensity was high enough, it dominated the shot peening coverage parameter.Yet if the intensity parameter was lower than the limit mentioned, earlier the correlation between shot peening coverage, residual stress and Barkhausen noise measurements was remarkable.

Tiivistelmä

Tässä pro gradu -tutkielmassa pyritään etsimään korrelaatiota kuulapuhallusparametrien, Barkhausenin kohinan vaihtelun, jäännösjännityksen, sekä jäännösausteniittipitoisuuden välillä. Barkhausenin kohinan mittauksella voidaan havaita jäännösjännityksen ja kovuuden vaihteluita mitattavassa ferromagneettisessa kappaleessa. Toisaalta jäännösjännityksen mittauksessa saadaan eksakti tulos pieneltä alueelta. Kuulapuhallus on eräs jälkityöstömetodi, jolla lisätään kappaleen pinnan kulutus- ja väsymiskestävyyttä. Työn tilaajana on toiminut Stresstech Oy ja tutkimuksessa on käytetty Scania AB:n valmistamia ja kuulapuhaltamia näytteitä, joista mitattiin Tampereen teknillisessä yliopistossa Barkhausenin kohinamittaukset, sekä röntgenmittaukset Stresstech Oy:n mittauspalvelussa.

Tutkimuksessa etsittiin erilaisilla metodeilla mahdollista korrelaatiota kuulapuhallusparametrien, Barkhausenin kohinasignaalin parameterien, jäännösjännityksen ja austeniittimittausten välillä. Erilaisia menetelmiä ja tuloksia käsiteltiin monia erilaisia, joista vain lupaavimmat on esitelty tässä tutkielmassa.

Käsitelty mittaustiedon määrä on hyvin laaja, joten jonkinlaista esikäsittelyä on järkevä tehdä. Mitattuihin syvyysprofiileihin sovitettiin toisen asteen polynomifunktio, rajoittaen mittaussyvyys 100 µm:iin. Saadun funktion kertoimia, pinta-alaa ja derivaatan nollakohtaa käytettiin itse korrelaatiotarkasteluissa. Monien vaiheiden jälkeen päädyin käyttämään monimuuttujaregressioanalyysiä, joka antoi lupaavimmat tulokset tässä työssä esitettyjen korrelaatioiden löytämisessä.

Mitattujen tulosten pohjalta merkittäviä korrelaatiota löytyi kuulapuhallusparametrien, röntgenmittausten tulosten, sekä Barkhausenin kohinan mittaustulosten välillä. Lisäksi havaitsin, että jäännösausteniittipitoisuudella ei ole kovinkaan suurta korrelaatiota muihin mittauksiin. Merkittävämpi havainto oli kuulapuhalluksen intensiteetin olevan dominoiva. Mikäli se oli liian intensiivinen, se dominoi kuulapuhalluksen peittoparametrin. Toisaalta mikäli intensiteetti oli alle löydetyn rajan, peittoparameterin korrelaatio jäännösjännitys ja Barkhausenin kohinan mittausten välillä oli merkittävä.

Table of Contents

1 Introduction

Throughout history, especially after industrial revolution, profit has been the top priority in manufacturing industry. Metal industry is not an exception. Cost efficiency is the key factor in manufacturing different components. To increase profits, the final product must cost as little as possible and it must be made as fast as possible. On the other hand, components and products need to be as durable enough to withstand all the abusive usage in their designed lifetime. Different process steps have their effect: the materials as well as the working and finishing methods each have their own impact on manufacturing processes and in the finished product. Materials should be chosen to be light, but the final surface should be as hard and durable as possible. There are multiple finishing methods to achieve these goals. In this thesis, the shot peening parameters are investigated, especially how shot peening parameter changes affect Barkhausen noise and X-ray diffraction measurement results.

Shot peening is a cold working process in which the sample surface is bombarded with hard spherical shots. During the shot peening the surface layer of the sample stretches and thus creates compressive stresses. In other words, compressive stress means that the material is in a denser state than in a stress-free surface, therefore improving resistance to abrasion and fatigue. Shot peening can also affect other material properties in the treated surface, for example by transforming retained austenite phase of iron into martensitic phase. The hardness of the surface layer can also increase due to the shot peening. When comparing different surface treatments, the shot peening method has its benefits: shot peening can increase component abrasion and fatigue resistance, and it is also an inexpensive surface treatment method. However, there are still some issues regarding shot peening, e.g. how shot peening parameters affect the treated samples. The most important parameters for shot peening are intensity and coverage which are further discussed in chapter 2.

One method to measure the ferromagnetic material properties is Barkhausen noise method. When an alternating magnetic field is induced locally into the sample, the magnetic field follows the hysteresis curve which contains small noise called as Barkhausen noise. This noise correlates into the changes of material stresses and hardness. Barkhausen noise method has its advantages, but also its disadvantages (see chapter 2).

The purpose of this thesis was to discover the correlation between the sample surface measurement results and shot peening parameters. Gear samples were utilized with different shot peening parameter treatment, in which both shot peening intensity and coverage were changed. The utilized measurements were: X-Ray based residual stress and retained austenite measurements, including depth profiles up to 0.5 mm, and magnetic Barkhausen noise measurement on the surface of the samples.

The outline of the thesis is as follows: first, I will begin by introducing the basic theory behind all the methods applied in the thesis (chapter 2). Next, I continue by describing the methods in more detail (chapter 3) followed by detailed an explanation of the utilized samples and measurement techniques (chapter 4). The results are then thoroughly presented in the following chapter (chapter 5). Finally, I conclude the thesis with a discussion of the results and ideas for further research (chapter 6).

2 Theory

In this chapter, I introduce all essential theoretical phenomena applied in this thesis. First the theory of the two utilized measurement methods, Barkhausen noise and X-ray diffraction, are explained. This is followed by sample treatment methods, and then theory regarding measurement result processing.

2.1 Barkhausen noise

Barkhausen noise, found by Heinrich Barkhausen in 1919, is the noise-like signal found in magnetic hysteresis curve (see e.g. ref. [5]). When a ferromagnetic sample is placed in an external varying magnetic field, the magnetic domain walls move and become trapped at pinning sites. When the domain walls break out of the pinning sites, it causes rapid and random movements which in turn cause the noise-like signal. The wall movements are influenced by material properties e.g. defects in material or changes in residual stresses.

2.1.1 Magnetic domains

Magnetic domains are small regions where magnetic spins are grouped and aligned [6]. Between these domains are domain walls, which are narrow zones of rapidly changing spin directions. When an external magnetic field is applied, the magnetic spins tend to turn into the direction of the external field. However, the spins act as a group when turning, instead of randomly turning alone. The magnetic domains that are already aligned with the external magnetic field expands, causing the movement of domain walls. Magnetic domains that are not aligned with the external magnetic field shrink as the aligned domains grow. A diagram is shown in Figure 1, in which the normal state of random oriented magnetic domains are presented on the left, and on the right are the same domains after having applied external magnetic field H.

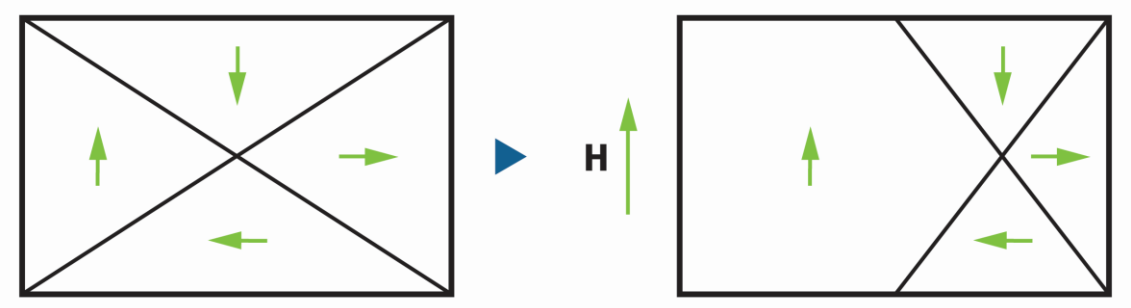

Figure 1 Magnetic domain movements in external magnetic field.

2.1.2 Barkhausen noise measurement method

Barkhausen noise method can be applied in practical measurements, specially when alternating magnetic field is utilized to change domain directions rapidly. This domain wall movement gives information of the ferromagnetic material properties.

When the Barkhausen noise method is utilized in practical measurements, the penetration depth of magnetization is commonly from 0.01 to 1.5 mm. This penetration depth depends on the magnetic properties of the material; typically, the studied materials are kind of alloys with ferromagnetic properties. The air-gap between the sensor and the studied surface is critical for the Barkhausen noise signal levels. In addition, the external magnetic field parameters need to be considered: current or voltage and frequency. When an alternating magnetic field is applied, the field strength can be controlled by voltage or current.

The penetration depth of Barkhausen noise is specified as the depth from where 67% (*1/e*) of the signal is present [7]. The Barkhausen noise signal depth can be estimated with the skin depth effect [8]. Skin depth effect explains how the amplitude of an electromagnetic wave incident upon a conductor. Electromagnetic wave decreases exponentially as a function of depth due to ohmic losses within the medium [8]. In the case of the incident magnetic field *B(z)*, the skin depth is given by [9]:

$$B(z) = Be^{-z/\delta},$$

where B is the initial amplitude, z is the depth into the conductor and δ is the skin depth, which represents the distance equal to a decrease in amplitude by a factor of *1/e.* The skin depth can be written as:

$$\delta = \sqrt{\frac{2}{\mu_0 \mu_r \sigma \omega}},$$

where μ_0 is permeability of free space, μ_r is relative permeability of the material, σ is specific electrical conductivity of the material, and ω is the angular frequency of the incident field.

2.1.3 Basics of a barkhausen noise sensor design

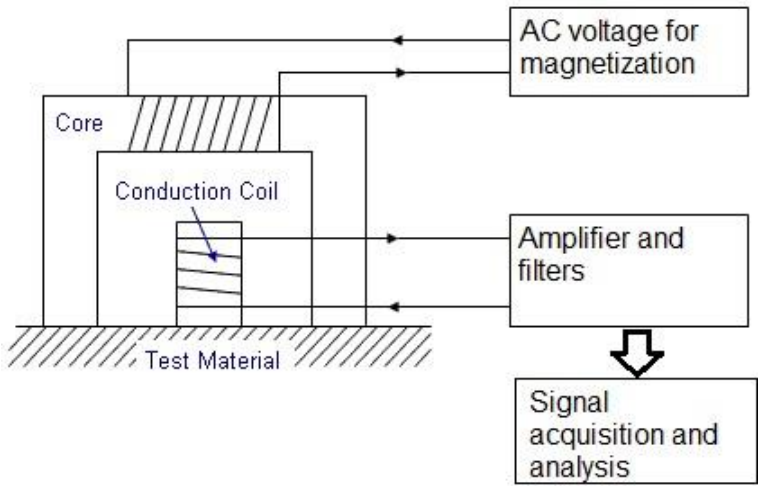

Figure 2 Basic sensor principle schematic for a Barkhausen noise sensor

Basic Barkhausen noise sensors (shown in Figure 2) have two magnetizing poles and one pick-up in between to detect the Barkhausen noise. In theory it's possible to leave the pick-up out and use band-pass filtering to filter out the unwanted magnetization signal. There are different types of pick-up designs as well, though the details are not that important regarding this thesis. It is also possible to add more pick-ups to detect the Barkhausen noise.

An AC current is applied to locally magnetize the studied sample. Magnetization direction changes in the sample and the magnetic domain wall movements cause Barkhausen noise signal, which is detected by the pick-up. This signal is amplified and sent into a data analyser which sends the data to the recording PC software.

2.2 X-ray diffraction

In this section, the theory behind X-ray diffraction based residual stress measurement method is explained in detail.

X-ray diffraction in crystallographic material research was an breakthrough in material study, as sample properties could be measured without destroying it. Wilhelm Röntgen discovered X-rays in 1895 [10] and in 1912 von Laue, Friedrich and Knipping passed X-rays through crystals of ZnS concluding that crystals are composed of periodic arrays of atoms and crystals cause distinct X-ray diffraction patterns due to atoms [11]. Only two years later in 1914, William Lawrence Bragg and his father Henry Bragg demonstrated that diffraction pattern can be utilized to determine relative positions of atoms within a single crystal, thus developing the Bragg's law which is the grounding theory in X-ray crystallography measurements [12].

2.2.1 Bragg's law

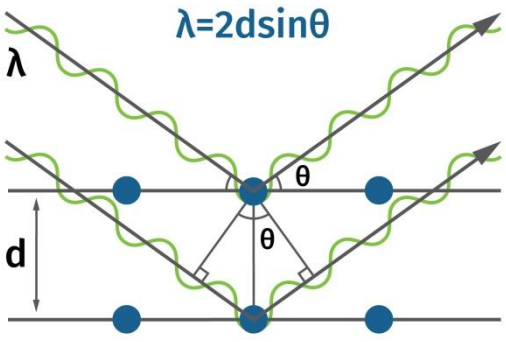

Figure 3 Relation between incident and reflective X-Ray beam. (Image courtesy of Stresstech Oy)

The relation between incident and reflective X-ray beams can be explained with Bragg's law, as shown in Figure 3. The incident and reflected beams have the same diffraction angle. Thus, the Bragg's law equation is:

$$n\lambda = 2d\sin\theta,$$

where n is a positive integer, λ is wave length, d is lattice plane distance and θ is diffraction angle, explaining how the relations are between the incident and reflection beams [13].

It needs to be noted that due to different atomic composition the diffraction angle θ is different for each material. The X-ray wavelength is selected so that the diffraction angle is as high as possible due to better sensitivity of d parameter. The lower diffraction limit is considered to be 130 degrees. This leads into a fact that it is beneficial to utilize different wavelength X-ray radiation for different materials.

2.2.2 Calculation of Residual Stress

X-ray diffraction is utilized to measure lattice plane distances. From this distance, it is possible to calculate residual stress of the material. Based on the Bragg's law, when a specimen is exposed to X-ray beam, the beam diffracts from crystal lattice causing a specific diffraction pattern. The diffraction peaks can be located by scanning through an arc above the specimen. When the specimen's stress level is not zero, it causes the diffraction pattern to move as the lattice plane distance d changes. The residual stresses move the diffraction peak patterns, and by measuring different ω or χ angles (Figure 4 and Figure 5) through the arc, the movement of the peaks can be detected [14]. This difference between the peaks of reference angle and other inclined angles can be utilized to calculate actual residual stress in the specimen. A more detailed description how to calculate residual stress of diffraction peak data can be found from [15].

There are different measurement modes in X-ray diffraction that can be applied in residual stress and retained austenite measurements. The two most common modes are: ω –mode and modified X mode [16].

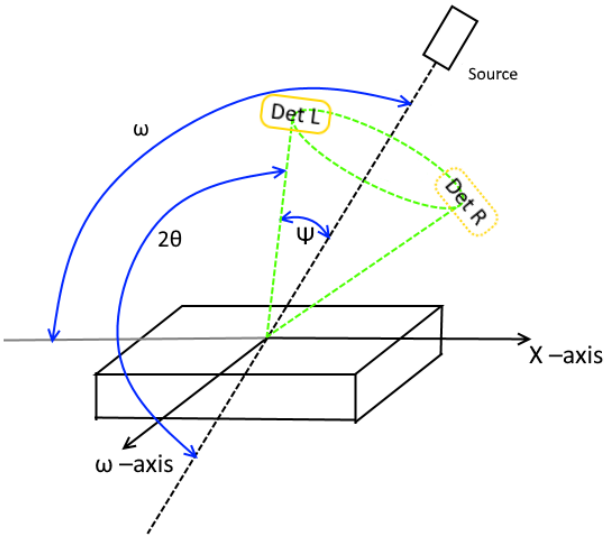

Figure 4 Schematic of ω –mode

The first presented mode is the ω -mode (Iso Inclination) method. In ω –mode the sample or diffractometer is rotated (tilted) around the ω –axis as shown in Figure 4. Both ω and 2θ axes are in the same plane. To obtain the ω -angle values, Ψ -angle values are mathematically added or subtracted to θ angles. It needs to be remembered that when calculating the θ –angles, and the Ψ –angle is positive, it is added to θ –angle and subtracted if Ψ –angle is negative. As a note, ω –mode can be measured with either one or two detectors.

The second method is the modified χ -mode where two detectors are usually utilized. The specimen is rotated around the χ -axis, which is normal to the plane containing ω and 2θ. At the *χ =0°* the incident beam is normal to the surface of the specimen, corresponding to ω=90°. The schematic of the modified χ –mode is shown in Figure 5. The benefit of using this modified method is to get double diffraction peaks at the same time, thus the result can be calculated as the average of the individual measurements from the two detectors. In theory, this modified χ -mode can be modified even more

with multiple detectors or even with large detector disc that can detect a complete diffraction cone.

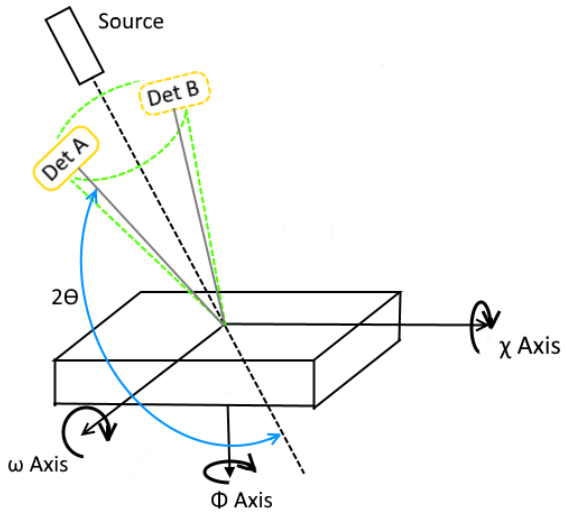

Figure 5 Schematic of modified χ –mode

2.2.3 Calculation of retained austenite content

X-Ray diffraction method can be utilized to find out for example different iron phases. In the industry, the amount of austenite in steel can sometimes become a problem as it is metastable. Austenite is a normal phase of steel in higher temperatures, yet in room temperatures austenite remains metastable. This means that in specific conditions the austenite transforms into martensitic. The transformation increases volume changes, causing higher compressive stresses inside the material which can lead into unwanted cracks in the specimen [17].

To measure retained austenite content in steel, X-ray diffraction can be applied. Martensite and austenite phases have different diffraction angles due to different lattice properties. Basic principle is that the larger diffraction peak of the phase means larger content of that phase in steel. Comparing the diffraction peak areas can directly give the amount of austenite phase in the steel sample. Different materials have multiple diffraction peaks; hence a so-called four peak austenite measurement is applied. In the four-peak method, the two first peaks of ferrite and austenite are utilized. When using this four-peak method, the third ferrite peak is so close to the second austenite peak that it needs to be blocked away with kβ -filter. See ref. [18] for more information regarding measurement of retained austenite content with X-ray diffraction.

2.3 Electropolishing

Electropolishing is applied in the industry to smoothen material surface. As the material is electro-chemically removed without heat, it does not affect residual stresses of the sample surface [19]. Thus it is very suitable in residual stress depth profile measurements as a method to remove material.

Electro polishing [20] is a similar process to electroplating [21], but in reverse. Instead of adding material, it is removed ion by ion. The metal object is connected into a DC power source positive terminal (anode), while another metal piece is connected into negative terminal of the same power source (cathode). When the anodic object and the cathode are immersed in an electrolyte solution, the electrolyte solution acts like a conductor to allow electricity flow between terminals. In the anodic sample the ions on the surface are oxidized and dissolved by being attracted towards the negatively charged cathode. Typically, the object surface is not perfectly smooth since it has microscopic peaks and valleys. Electric fields are concentrated into these peaks, increasing the local removing rate over that of the valleys and resulting into smoother surface on the object [22].

When altering the setup slightly instead of immersing anode and cathode into a solution pool, the electro polishing area can be reduced: this allows more controlled material removal for residual stress depth profile measurements. Solution area can be limited with a nozzle which is in direct contact to the object and it is surrounding the cathode. The removed material amount can be measured for example with a dial indicator. Based on several researches, it is one of the best alternatives in material removal regarding residual stress depth profile measurements which study shot peened samples [23].

2.4 Shot peening process

Manufacturing quality and cost benefits are the key words in modern industry [24]. One way to get denser surface on metal parts is the shot peening treatment [25]. As the name suggests, small spherical metal particles, shots, are bombarded into the sample. Every shot acts like a tiny peening hammer, compressing the sample surface structure generating compressive stress underneath the surface. If only a few shots are applied, the sample surface becomes uneven and the stress levels vary immensely on a small area. This causes low fatigue resistance due to varying stress levels on the part surface. If there are plenty of shots, yet the kinetic energy of a shot is low, the sample surface is nice and even; however, the low energy shots do not cause high enough compressive stresses into the sample, which also means low fatigue resistance [26]. The problem is to determine a good compromise with the shot peening parameters to ensure good quality shot peening. There are two key parameters in shot peening: Almen intensity (mmA) and coverage (kg/cm^2). Intensity is given by Almen intensity [27], which is defined as the calculated Almen strip arc height at which doubling the peening time yields (only) 10% increase in arc height.

The definition of coverage parameter applied in this thesis deviates slightly from the industrial norm of SAE-J2277, in which coverage is defined as the percentage of a surface that has been impacted by the peening media. The minimum peening time required to obtain 100% coverage is determined by gradually increasing total peening time until the entire peened surface exhibits overlapping dimpling. Coverages above 100% are multiples of the exposure time required to achieve 100% coverage. Coverage over 100% cannot be visually inspected by the methods described here; instead this thesis defines coverage as a coverage "density":

$$Coverage\ density = \frac{CT.n.F}{S},$$

where CT: Total peening time [s], n: total number of nozzles [-], F: Media flow per nozzle [kg/s] and S: Area to be peened [cm^2].

In addition, the shot size and weight affect the treatment effect. It also needs to be noted that too excessive shot peening increases compressive stresses, which may lead into decreasing fatigue resistance.

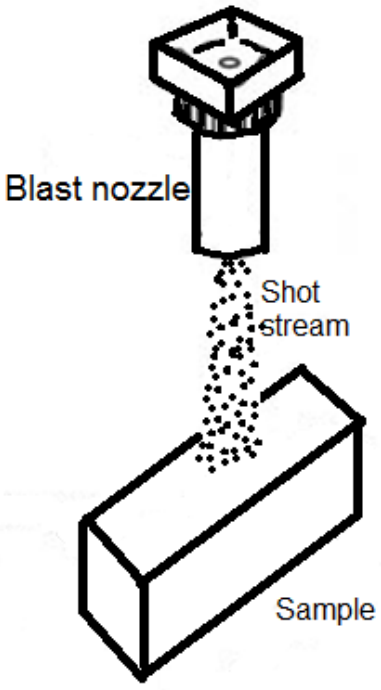

Figure 6 Shot peening process schematic.

2.5 Multiple linear regression analysis

Multiple linear regression analysis is a powerful technique utilized for predicting the unknown value of a variable from the known value of two or more variables [28]. Only two types of variables are needed; dependent and independent variables. Dependent variable is predicted in the model, while independent variables are utilized to predict the dependent variable. Multiple linear regression analysis is based on a simple equation of Y and $X_1, X_2 \ldots X_k$, where Y is the dependent variable and X_i are independent variables. The equation for multiple linear regression model in general form is:

$$Y = b_0 + b_1X_1 + b_2X_2 + \cdots + b_kX_k,$$

where b_0 is the intercept and $b_1, b_2,\ldots,b_k$ are analogous to the slope in linear regression equation, also called regression coefficients. As an example, when only one independent variable X_i is utilized, in which if b_1 is 2.5 then if Y increases 2.5 units, then X_1 increases with 1 unit.

One question remains, how to test the appropriateness of the multiple regression model and its reliability. Typically, the appropriateness is tested with the F-test [29]. A significant F indicates a linear relationship between Y and at least one of the X's. With this test, it is possible to leave unnecessary variables out from the equation and concentrate only on the meaningful variables. On the other hand, the goodness of predicting Y is given by R^2 coefficient [30]. The R^2 runs between [0,1], where 0 is zero relation and 1 means complete relation. Though if more than one X is utilized, adjusted R^2 can be utilized instead. The adjusted R^2 coefficient is calculated as follows:

$$R^2_{adj} = 1 - \left[\frac{(1-R^2)(n-1)}{(n-k-1)}\right],$$

where n is the number of observations utilized in regression and k is the number of X variables.

When utilizing multiple regression analysis, there is one matter to consider when interpreting results: they give usually standard error. The error term represents the combined effect of the omitted variables. This error term should not be mixed with the standard error of Y itself, or with the standard errors of regression coefficients [32].

3 Experimental methods

In this chapter I present all the details regarding applied experimental methods. I start by explaining how Barkhausen noise method was used in measurements. Next, I describe how X-ray diffraction method was utilized. Lastly, shot peening parameters and setup are explained in more detail.

3.1 Barkhausen noise in measurements

The ideal solution is that samples could be measured without destroying them in the process. Measurement methods can be divided into two groups: Non-Destructive methods (NDT-methods) and Destructive methods (DT-methods). With NDT-methods, all the production can be measured and then divided into good and bad specimens. Barkhausen noise method is an NDT-method: it uses single probe which is recommended to be in contact with the specimen surface. There is no requirement for cutting or marking the specimen, nor any requirement for acid treatments. Barkhausen noise measurements can be made dynamically by either moving the probe or the specimen.

The disadvantage of Barkhausen noise measurements is the contact between the specimen and the probe as even the smallest air-gap can affect the results. Therefore, as the specimen geometry changes, the sensor geometry also must change also. A general-purpose sensor exists as well, yet it cannot be utilized in dynamic measurements due to the sensor structure. Even though most of the applications can be measured with general type sensors, nowadays a sensor can be shaped into any three-dimensional continuous surface. One good example is a cam shaft sensor, which can be utilized to measure all kinds of continuous cylindrical specimens that are rotated in tangential direction around the primary axis. Other typical sensor types are gear flank and root sensors that can be utilized to measure different types of gears, such as straight or even helix-angled. Some specimen surfaces are so small that it is physically impossible to fit magnetization poles and a pick-up in the same area, leaving only one option: using magnetization which is produced with a large magnetization yoke.

The Barkhausen noise measurements in this project were made with a handheld flank sensor and a Rollscan 300 Barkhausen noise analyser, shown in Figure 7. MicroScan software [33] was used in data recording. The software calculates many parameters from the measured data, which are tabulated in Table 1. An example graph of a Barkhausen noise burst is shown in Figure 8.

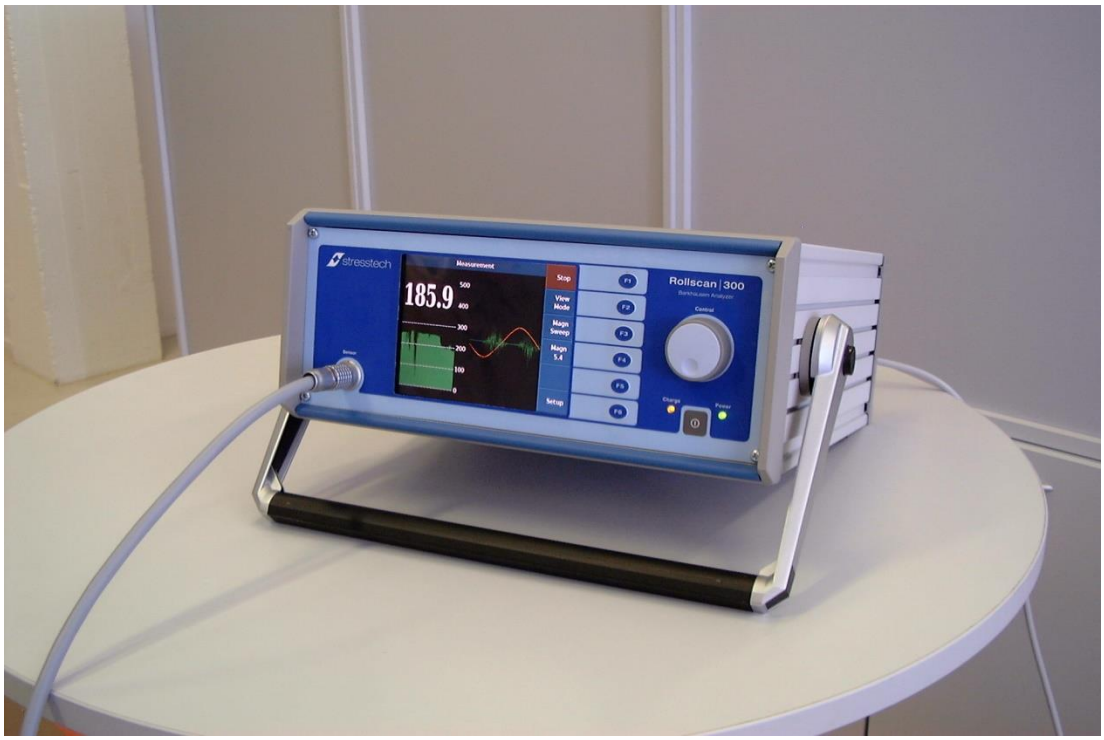

Figure 7 RollScan 300 device.

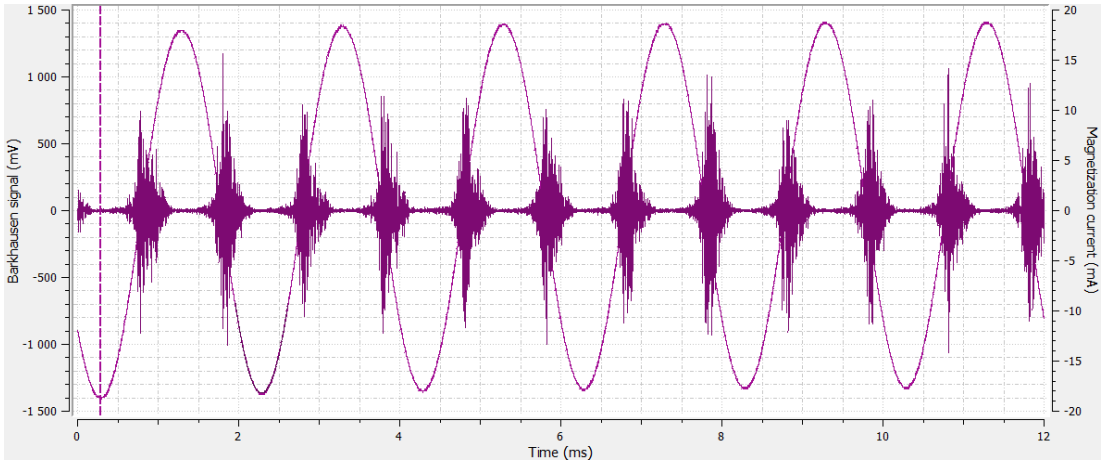

Figure 8 Example graph of MicroScan software showing Barkhausen noise burst.

Table 1. MicroScan software parameters and explanations

Parameter	Explanation
RMS (average, positive and negative) [mV]	Root Mean Square value of the Barkhausen noise signal
Peak value (average, positive and negative) [mV]	Barkhausen noise signal peak values
Peak position (average, positive and negative) [ms]	Barkhausen noise signal peak position
FWHM (average, positive and negative) [ms]	Full Width at Half Maximum value of the Barkhausen noise signal peak
Coercivity [kA/m]	Integrally calculated coercivity value, which describes the ability of a ferromagnetic material to withstand an external magnetic field without becoming demagnetized
Remanence [T]	Remanence value, which is integrally calculated and describes the amount of magnetization retained into sample after an external magnetization field is removed
Permeability [μ]	Integrally calculated permeability value describing the degree of magnetization of a material in response to a magnetic field
x Area [mVs]	Integral area of a Barkhausen noise burst
Spectrum Area [mVs]	Spectrum area of a Barkhausen noise burst

3.2 Residual Stress and Retained Austenite measurements with X-ray diffraction

X-ray device consists of X-ray Main Unit (XMU), diffractometer, X-ray tube and detectors. An example setup is shown in Figure 9. The main unit produces high voltage, up to 30 kV, as well as cooling for the X-ray tube. Diffractometer handles all the movements that is required in measurement, and it can for

example be replaced by a high accuracy robot which enables more freedom for movement. Detectors are attached underneath the X-ray tube to capture the diffracted X-rays. The X-rays are guided from the X-ray tube through a collimator, which focuses X-rays into a smaller area from 0.3 to 5mm diameter, or even slit collimators can be utilized. To get more precise results compared to ω -mode measurements, residual stress measurements were measured in modified χ –mode shown in Figure 10. Retained austenite measurements were measured in ω -mode, using a four-peak measurement shown in Figure 11. This modified ω -mode was used because of physical limitations of fitting two detectors on a single arc.

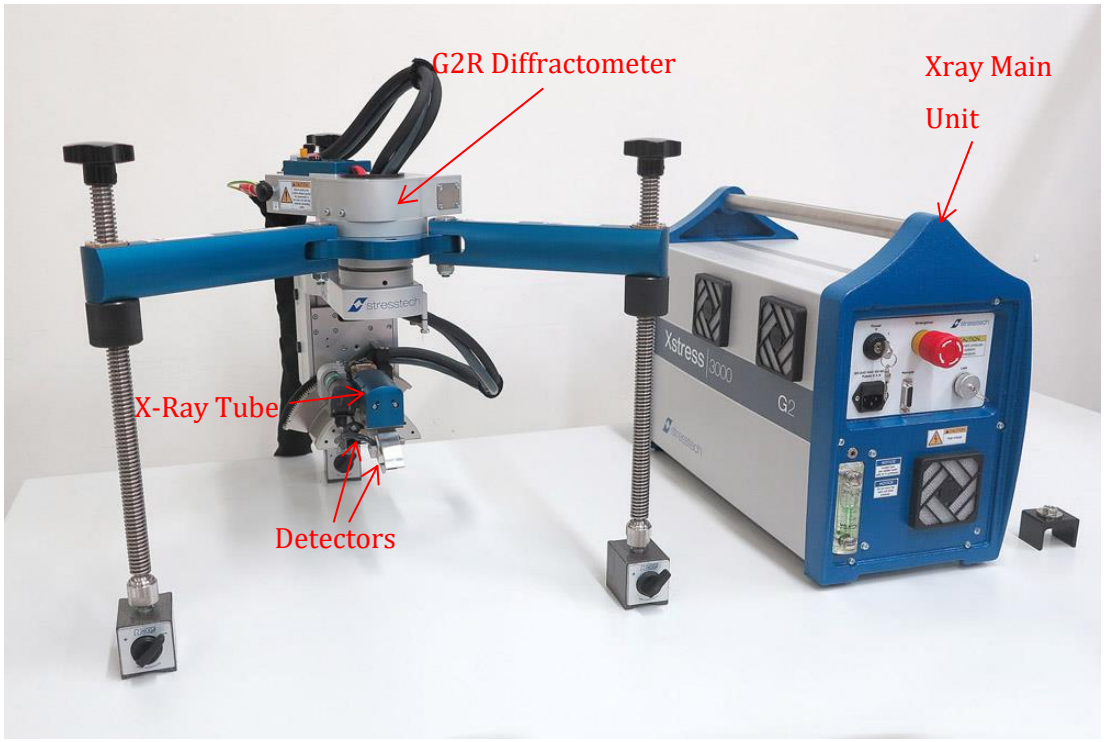

Figure 9 G2R Diffractometer system and the names of the parts

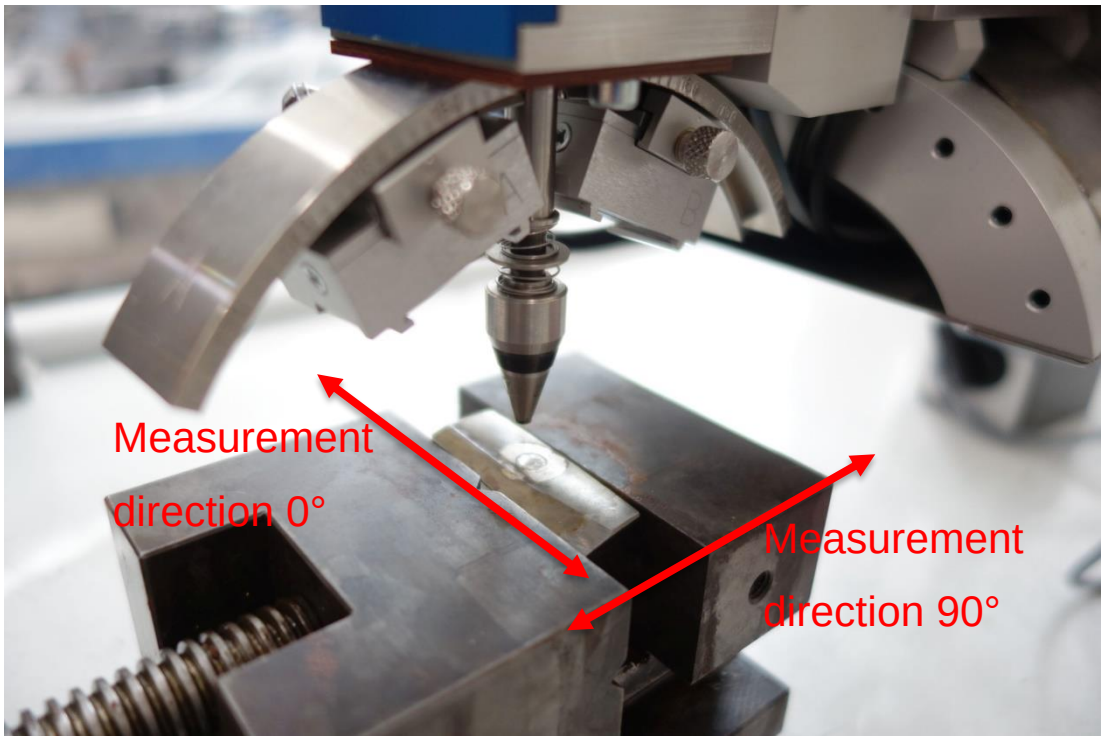

Figure 10 Residual Stress measurement setup with measurement directions

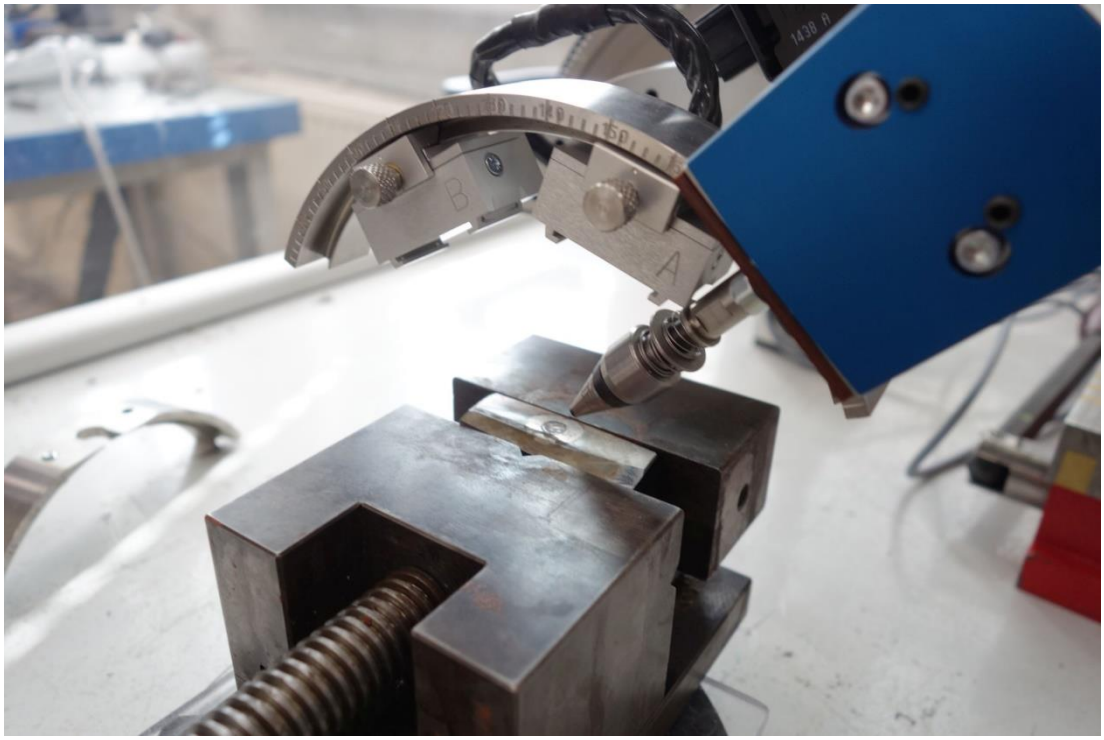

Figure 11 Retained Austenite measurement setup

X-rays are produced by using a current to heat a filament which emits electrons by thermionic emission; electrons are accelerated by high voltage. They collide into a specific material target, creating characteristic X-ray radiation which is guided through a beryllium window. X-ray tube creates plenty of heat and therefore cooling is required. A simple X-ray tube schematic is shown in Figure 12.

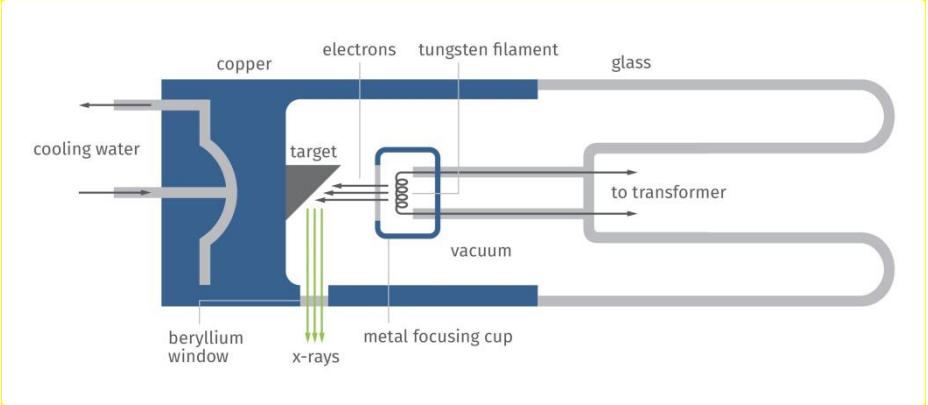

Figure 12 Schematic diagram of an X-ray tube (Image courtesy of Stresstech Oy)

3.3 Utilized shot peening process parameters

The total number of different parameter setups in shot peening was 14. Parameters included 6 different intensity levels and 5 coverage levels. Shot peening parameter test setup is shown in Figure 13.

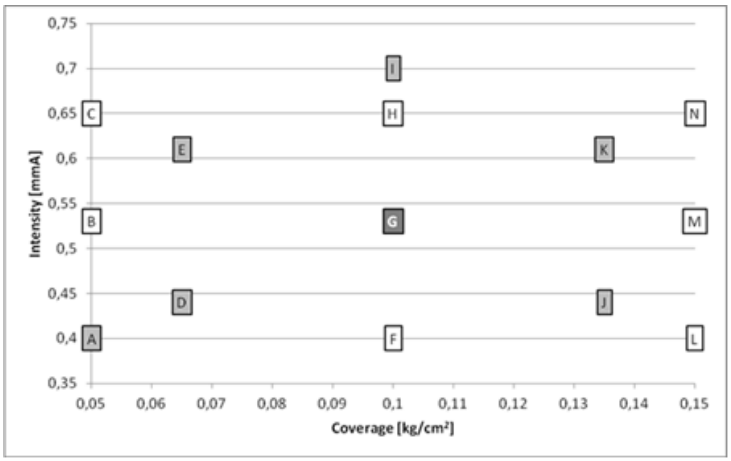

Figure 13 Shot peening test setup graph of Intensity vs Coverage.

More specifically, shot peening parameters are tabulated in Table 2, in which the trial designation is shown for result handling.

Table 2. Measured sample Shot peening parameters and given labels

Label	Trial	Coverage	Intensity
A	SG23	0.05	0.4
B	SG17	0.05	0.53
C	SG13	0.05	0.65
D	SG12	0.065	0.44
E	SG18	0.065	0.61
F	SG20	0.1	0.4
G	SG11	0.1	0.53
H	SG8	0.1	0.65
I	SG9	0.1	0.7
J	SG3	0.135	0.44
K	SG4	0.135	0.61
L	SG15	0.15	0.4
M	SG6	0.15	0.53
N	SG19	0.15	0.65

4 Experiments

4.1 Measured samples

One sample of each shot peening group was selected for Barkhausen noise and X-ray measurements. The total number of studied samples was 14, each of which were treated with different shot peening parameters. In order to conduct X-ray measurements on a tooth flank, a couple of the teeth were cut from the gears.

4.2 Barkhausen noise measurements

Barkhausen noise measurements were conducted with a handheld sensor on each intact flank, and the average of results have been utilized in the correlation calculations. The Barkhausen noise measurements were carried out by Suvi Santa-Aho [34]: the test setup is shown in Figure 14.

Figure 14 Barkhausen noise measurement test setup: left flank measurement on the left and right flank measurement on the right. Measurements wereconducted with an axial magnetization direction.

Barkhausen noise measurements were done with magnetization frequency of 200 Hz in axial direction.

4.3 Residual stress and retained austenite measurements

The samples' residual stress and retained austenite depth profiles were measured with intended depths of 0, 5, 10, 30, 50, 75, 100, 150 and 200 µm, continuing with 50 µm steps. This was done until the stress values stabilized. Example graphs of residual stress, FWHM and Retained austenite measurement results are shown in Figure 15, Figure 16 and Figure 17. Samples were measured on the surface, then the desired layer was electropolished off. To guarantee reliable results, the depths were measured with a dial indicator before and after measurement.

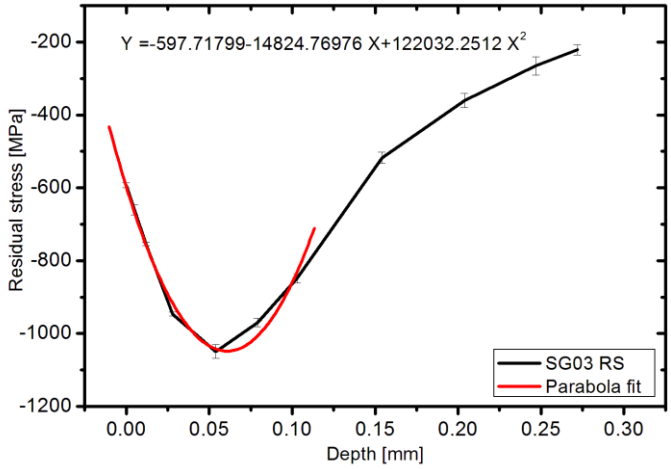

Figure 15 Example figure on an SG03 residual stress depth profile in 0° direction, where the 0° direction refers to a parallel direction to gear flank edge. Also shown is a fitted parabola up to ~100 µm and a parabola equation.

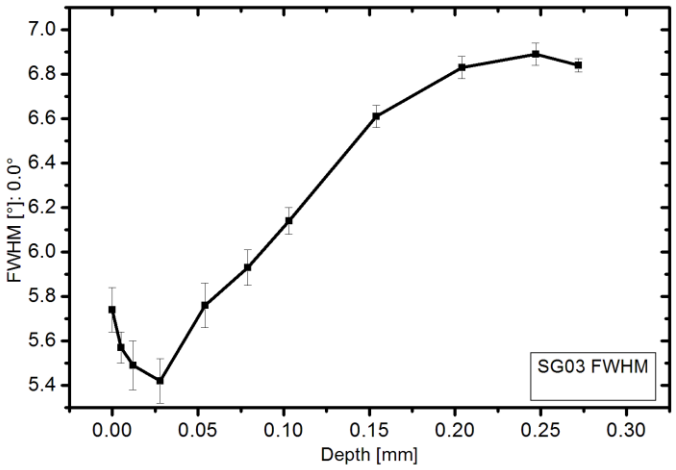

Figure 16 Example figure on an SG03 FWHM depth profile in 0° direction.

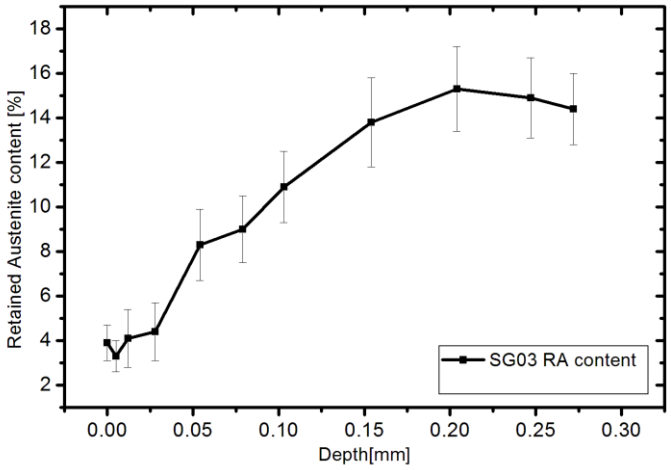

Figure 17 Example figure on an SG03 retained austenite depth profile in 0° direction.

5 Results

5.1 Measurement results

As described earlier, MicroScan software delivers a total of 17 parameters. On each residual stress measurement, two different parameters are produced: stress in MPa and *FWHM* in degrees, with all the values in two directions. In order to evaluate the residual stress depth profile, a 2nd order polynomial was fitted to the residual stress depth profiles counting only depths up to ~100 µm, and using a parabola equation:

$$y = ax^2 + bx + c,$$

where *y* and *x* are Cartesian coordinates, and *a, b* and *c* are polynomial coefficients. Correlation calculations included all the MicroScan parameters, retained austenite content on the surface and key parameters of the 2nd order polynomial of residual stress measurements. The key parameters are: *a, b, c* of 2nd order polynomial, polynomial *Area* and *Derivative zero point* i.e. the position of the lowest value point of the parabola. The lowest value point of the parabola is a parabolic approximation of the highest residual stress level found in the measurement. Measurement data values are shown in Appendix 1.

5.2 Correlation between the measurements

Correlation results are shown in from Figure 18 to Figure 24, and are tabulated from Table 3 to Table 9. In the figures and tables, correlation parameters are written in captions, in which terms *X*×*Y* mean that that it is the product of *X* and *Y*.

The retained austenite measurements did not give any good correlation into any experiments.

5.2.1 Correlation between Shot peening intensity, Barkhausen noise measurements and Residual Stress measurements

The correlation between shot peening intensity and the highest residual stress level can be found in Figure 18, and the regression statistics are tabulated in Table 3. From these results, a good correlation can be found with shot peening intensity and highest residual stress level. Based on this result the shot peening intensity correlates well with highest residual stress levels. There is some variance in the results, and one of the reasons for this variance could be parabolic approximation of the stress profile up to 100 µm. Variance could be caused by uniformity of the shot peening process, how well the process is repeatable, and residual stress depth profile measurement.

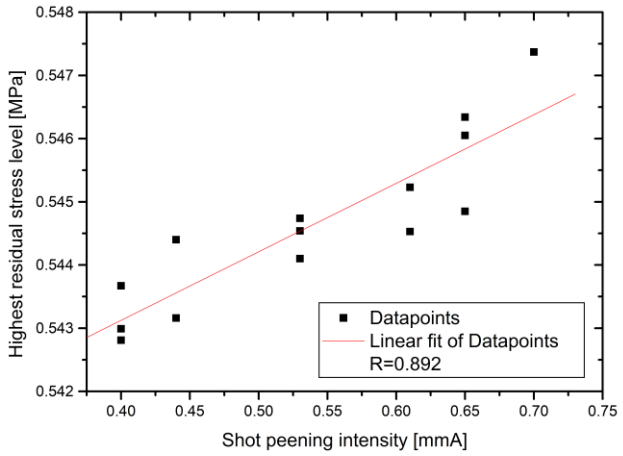

Figure 18 Correlation plot of the shot peening intensity and the highest residual stress level

Table 3. Correlation results between the shot peening intensity and the highest residual stress level

Multiple R	0.892
Adjusted R^2	0.778
Standard Error of the estimate [MPa]	0.051
Number of observations	14

The highest residual stress level can be correlated with multiple regression function into parameters, which are calculated from the Barkhausen noise level. The result of this shown in Figure 19, and statistics in Table 4. The parameters which give good correlation into highest residual stress level are: Peak position average, Coercivity, Permeability, Peak position average × Coercivity and Peak position average × Permeability. The amount of correlated Barkhausen noise parameters is quite high, which is one reason why more studies are needed to find the most important parameters for correlation. There is plenty of variance in the middle region in the Figure 19, this variance doesn't affect the correlation that much. To get better understanding of the correlation, the samples need to have higher and lower shot peening intensity. As previously found, the shot peening intensity has direct effect into residual stress levels in the studied samples.

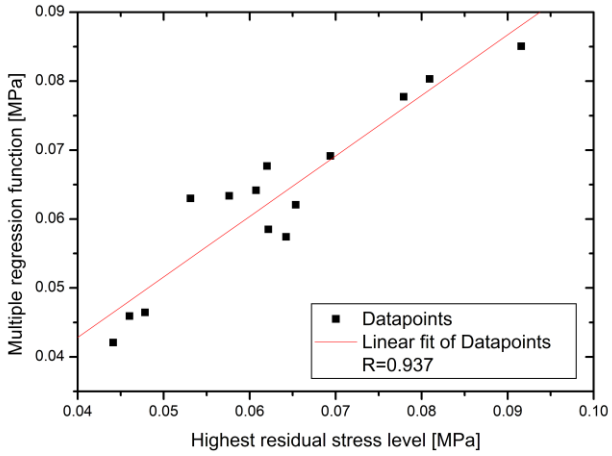

Figure 19 Correlation plot of the highest residual stress level and the multiple regression function, including the parameters: Peak position Avg, Coercivity, Permeability, Peak pos. Avg.× Coercivity and Peak pos. Avg. × Permeability

Table 4. Correlation statistics between the highest residual stress level and the multiple regression function including the parameters: Peak position Avg, Coercivity, Permeability, Peak pos. Avg.× Coercivity and Peak pos. Avg. × Permeability

Multiple R	0.937
Adjusted R^2	0.802
Standard Error of the estimate [MPa]	0.006
Number of observations	14

Correlation results between shot peening intensity and Barkhausen noise parameters can be found in Figure 20 and statistics in Table 5. When correlating shot peening intensity directly into parameters derived from Barkhausen noise, the number of needed parameters is much smaller to get good correlation. Based on these results, there is a correlation between shot peening intensity, highest residual stress levels and magnetic properties of the material.

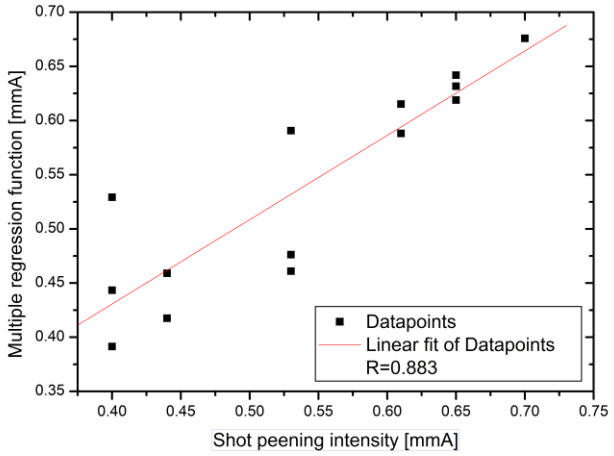

Figure 20 Correlation plot of the shot peening intensity and the multiple regression function including the parameters: Peak position Average, Coercivity and Permeability

Table 5. Correlation statistics between the shot peening intensity and the multiple regression function including the parameters: Peak position Average, Coercivity and Permeability

Multiple R	0.883
Adjusted R^2	0.713
Standard Error of the estimate [mmA]	0.058
Number of observations	14

5.2.2 Correlation between Shot peening coverage and Barkhausen noise and Residual stress measurements

When correlating Shot peening coverage, it was discovered that if shot peening intensity is too high then no correlation can be found. After numerous calculations, the maximum limit for shot peening intensity in this measurement setup was discovered to be 0.5 mmA. When the shot peening intensity was below that particular limit, the correlation between coverage, residual stress and Barkhausen noise measurements was remarkable. Results with the intensity below 0.5 mmA have been chosen, only 5 samples which are good enough for preliminary correlation calculations.

The correlation between shot peening coverage and residual stress depth profile parabola area is good, as shown in Figure 21 and in the statistics in Table 6. One explanation for this good correlation is that shot peening coverage is basically how many shots are bombarded in a certain area. As described previously, the shot peening intensity has direct correlation with the highest residual stress

level. Based on this finding, we can conclude that when the shot peening coverage is higher, the shot peening effect penetrates deeper into the sample material as the approximation parabola area is larger.

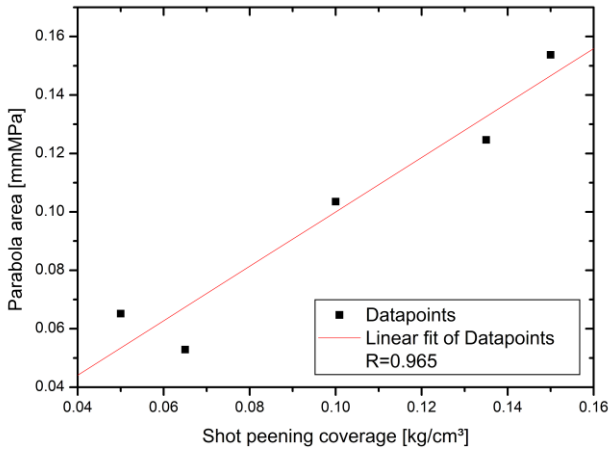

Figure 21 Correlation plot between the shot peening coverage (when the shot peening intensity [mmA] is <0.5) and yhe parabola area of the residual stress depth profile

Table 6. Correlation statistics between the shot peening coverage (when the shot peening intensity [mmA] is <0.5) and the parabola area of the residual stress depth profile

Multiple R	0.965
Adjusted R^2	0.909
Standard error of the estimate [mmMPa]	0.013
Number of observations	5

Correlation findings between residual stress depth profile estimation parabola area and Barkhausen noise parameters can be found in Figure 22, and the statistics in Table 7. The standard error of the estimate is presented in the statistics: it is quite high compared to previous correlation calculations. The higher standard error can be explained with a low amount of observations, when an observation deviates from the average its effect on standard error is high. Even though the standard error is quite high, there is still good correlation between the parabola area and the magnetic properties of the sample.

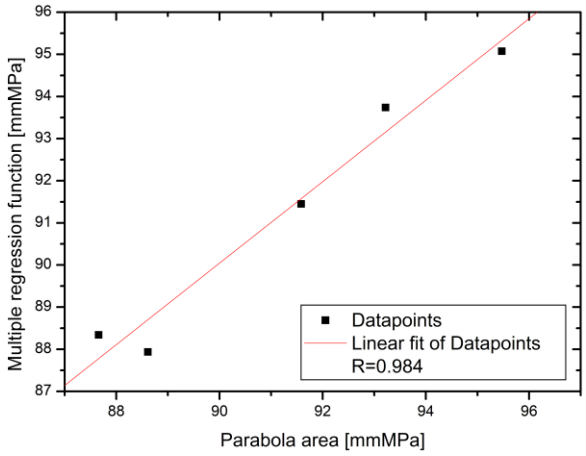

Figure 22 Correlation plot between the parabola area (when the shot peening intensity [mmA] is <0.5) and the multiple regression function including the parameters: FWHM average and coercivity

Table 7. Correlation statistics between the parabola area (when the shot peening intensity [mmA] is <0.5) and the multiple regression function including FWHM average and coercivity

Multiple R	0.984
Adjusted R^2	0.935
Standard error of the estimate [mmMPa]	0.826
Number of observations	5

The result of direct correlation between shot peening coverage and derived parameters from Barkhausen noise is shown in Figure 23, and the statistics are tabulated in Table 8. This correlation is so good that it is suspicious: even the standard error of the estimate is almost zero. The correlation was examined so that each variable was removed one by one, yet the correlation remained just as high with all the variables – therefor it can be said that the correlation result is reliable. In order to investigate goodness of the fit, further studies with improved test setup are needed.

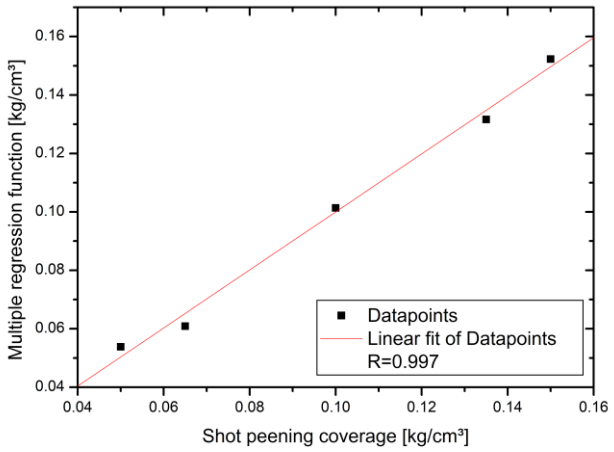

Figure 23 Correlation plot between the shot peening coverage (when the shot peening intensity [mmA] is <0.5) and the multiple regression function including parameters: FWHM average and coercivity

Table 8. Correlation statistics between the shot peening coverage (when the shot peening intensity [mmA] is <0.5) and the multiple regression function including parameters FWHM average and coercivity

Multiple R	0.997
Adjusted R^2	0.987
Standard error of the estimate [kg/cm³]	0.005
Number of observations	5

5.2.3 Correlation between shot peening intensity and residual stress measurements on the surface

When correlating shot peening intensity with only surface residual stress measurements, the result is not as encouraging as shown in Figure 24 and in the statistics in Table 9. The measurement directions

are the same as in the example in Figure 10. This result is important because it confirms that to get better understanding how well the shot peening process is carried out, it is necessary to make depth profile with XRD-based measurements.

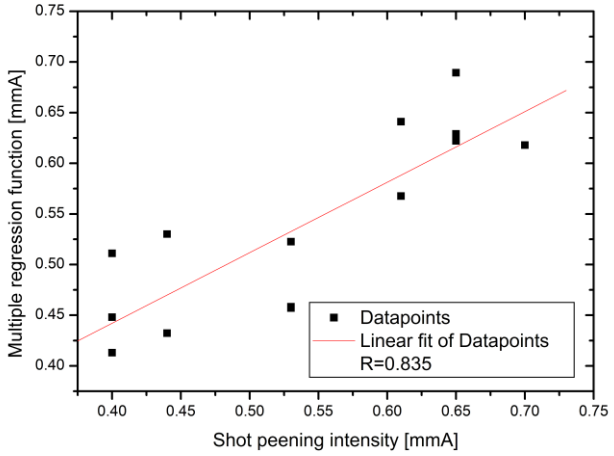

Figure 24 Correlation plot between the shot peening intensity and the multiple regression function including the parameters: residual stress on surface measurement of 0° and 90° directions and the cross term 0° × 90°.

Table 9. Correlation statistics between the shot peening intensity and the multiple regression function including the parameters: residual stress on surface measurement of 0° and 90° directions and the cross term 0° × 90°

Multiple R	0.835
Adjusted R^2	0.605
Standard error of the estimate [mmA]	0.068
Number of observations	14

There was no correlation found in measurements of shot peening coverage and surface residual stress.

6 Discussion

A correlation can be found between shot peening parameters, X-ray based residual stress measurements and Barkhausen noise measurements. One of the goals of this study was to find a correlation chain in shot peening parameters to X-ray based measurements, then continue to Barkhausen noise measurements. Another goal was to examine direct correlation between shot peening parameters and Barkhausen noise measurements. Both goals were accomplished with good correlation; however, it needs to be noted that, based on the correlation calculations, the initial shot peening parameters could be improved.

The direct correlation between shot peening parameters and Barkhausen noise measurements gave higher correlation than the one between X-ray diffraction and Barkhausen noise measurements. The conclusion for this finding is that there is always some error left in the practical measurements and the utilized methods. The second, perhaps even more important key finding is that the shot peening intensity dominates the shot peening coverage after it reaches a certain limit. This is understandable as the shot peening coverage basically means the amount of shots in particular area. Shot peening intensity is analogous to the velocity of the shot when it impacts the sample surface. As the shot has higher velocity, it causes larger deformative dimple on the sample surface which leads to higher residual stress levels under the sample surface. If the shot peening intensity is under the found limit value, the shot peening coverage causes the shot peening effect to penetrate deeper into sample material. However, this latter finding needs further research as there were only a few samples with low enough shot peening intensity.

The current project has been limited by the number of shot peened samples and different parameters, since it was found that the shot peening intensity can be dominating over the shot peening coverage. Another limiting factor was the utilized approximation function which simplifies the residual stress depth profile measurements. The used parabola function was applied for its simplicity as the function terms are easy to understand and apply in multiple regression analysis.

This thesis answered some questions regarding the correlation between the results of shot peening parameters, X-ray diffraction measurement and Barkhausen noise measurement results. The next step in further research would be to improve shot peening parameter setup, with more samples of low enough shot peening intensity. The key correlation parameters are known based on the findings in this project, therefor another improvement idea is to utilize more complex and accurate approximation function to residual stress depth profile measurement results. For further research, the shot size could be studied as well. As the shot is larger, it has more kinetic energy: is it possible to have the same effect with larger shots with lesser intensity? Barkhausen noise measurement setup could also be improved,

as it was made with a handheld sensor. –Nowadays there are fully automatic measurement machines which have really good repeatability. In conclusion, the thesis is only a scratch on the surface when studying the effects of shot peening on metallographic samples.

References

[1] Mechanical Engineering, Hot and Cold working processes (28.6.2016). Retrieved from: http://engineeringhut.blogspot.fi/2010/10/hot-and-cold-working-processes.html

[2] Frank Petit-Renaud, Optimization of the Shot Peening parameters. USF Impact Finishers (Shot Peening division) and USF Vacu-Blast International

[3] Dong-Sun Lee, Tae-Hyung Kim, Jae-Heon Lee, Tae-Kun Lee and Seong-Kyun Cheong, A Study on the Improvement of Durability of Gear Streel by Shot Peening. Trans Tech Publications, Switzerland

[4] Wolfram Math World, Full Width at Half Maximum (21.7.2016). Retrieved from: http://mathworld.wolfram.com/FullWidthatHalfMaximum.html

[5] Stresstech Group, Barkhausen noise analysis (20.2.2017) Retrieved from: http://www.stresstech.com/en-fi/products/barkhausen-noise-equipment/barkhausen-noise-analysis/

[6] University of San Diego, Magnetic domains (9.6.2016). Retrieved from: http://magician.ucsd.edu/essentials/WebBookse21.html

[7] Chih-Wen Chen, Magnetism and Metallurgy of Soft Magnetic Materials. Amsterdam; New York; North-Holland Pub. Co., 1977. (Series of monographs on selected topics in solid-state physics ; 15)

[8] Paul McNairnay, Magnetic Barkhausen Noise Measurements Using Tetrapole Probe Designs. Queen's University, Kingston, Ontario, Canada, 2014.

[9] D. J. Griffiths, Introduction to Electrodynamics Third Edition. Prentice Hall, 1999.

[10] Nobelprize, Wilhelm Conrad Röntgen – Biographical (28.6.2016). Retrieved from: http://www.nobelprize.org/nobel_prizes/physics/laureates/1901/rontgen-bio.html

[11] Ewald, P. (1962), *Fifty Years of X-ray Diffraction*, Utrecht: Oosthoesk's Uitgeversmaatschappij.

[12] California Institute of Techology, A short history of x-rays (28.06.2016). Retrieved from: http://authors.library.caltech.edu/5456/1/hrst.mit.edu/hrs/materials/public/X-rays/diffraction.htm

[13] B. D. Cullity, Elements of X-Ray Diffraction, Second Edition.

[14] Cambridge physics, X-Ray diffraction (23, February 2016). Retrieved from: http://www-outreach.phy.cam.ac.uk/camphy/xraydiffraction/xraydiffraction7_1.htm

[15] M.E. Fitzpatrick, A.T. Fry, P. Holdway, F.A. Kandil, J. Shackleton and L. Suominen, Measurement Good Practice Guide No. 52; Determination of Residual Stres by X-ray diffraction – Issue 2

[16] ASTM International, Standard E2860 (30, April 2016). Retrieved from: http://www.astm.org/Standards/E2860.htm

[17] Daniel H. Herring, A discussion of Retained Austenite. The Heat Treat Doctor: www.heat-treat-doctor.com

[18] ASTM E975 - 13 Standard Practice for X-Ray Determination of Retained Austenite in Steel with Near Random Crystallographic Orientation

[19] Rasha Alkaisee and Ru Lin Peng, Influence of Layer Removal Methods in Residual Stress Profiling of a Shot Peenend Steel using X-ray diffraction. Advanced Materials Research Vol 996 (2014).

[20] Process Stainless Lab Inc, What is Electropolishing? (1.7.2016). Retrieved from: http://www.pslinc.com/what-electropolishing

[21] Ken Osborne, Electroplating. Metal Protection Ltd, Auckland

[22] ASTM E1558-09, Standard Guide for Electrolytic Polishing of Metallographic Specimens, ASTM international 2009

[23] Dr. Jian Lu, Handbook of Measurement of Residual Stresses.

[24] Harry Chandler, Metallurgy for the Non-Metallurgist, ASM International, 1 Mar 1998.

[25] Curtis Wright, Shot peening (14, March 2016). Retrieved from: http://www.metalimprovement.com/shot_peening.php

[26] Lamda technologies, Shot peening (23, February 2016). Retrieved from: http://www.lambdatechs.com/shot-peening.html

[27] Intensity of shot peening, OSK Kiefer GmbH (12.7.2016). Retrieved from: http://osk-kiefer.de/wp-content/uploads/28-definition_of_shot_peening_control_and_parameters_go.pdf

[28] School of public health, Multiple linear Regression Analysis (15, April 2016). Retrieved from: http://sphweb.bumc.bu.edu/otlt/MPH-Modules/BS/BS704_Multivariable/BS704_Multivariable7.html

[29] The Minitab Blog, Understanding Analysis of Variance (ANOVA) and the F-test (29.6.2016). Retrieved from: http://blog.minitab.com/blog/adventures-in-statistics/understanding-analysis-of-variance-anova-and-the-f-test

[30] The Minitab Blog, Regression analysis: How Do I Interpret R-squared and Asses the Goodness-of-Fit? (29.6.2016). Retrieved from: http://blog.minitab.com/blog/adventures-in-statistics/regression-analysis-how-do-i-interpret-r-squared-and-assess-the-goodness-of-fit

[31] The Minitab Blog, Multiple Regression Analysis: Use adjusted R-squared and Predict R-squared to Include the Correct number of variables (29.6.2016). Retrieved from: http://blog.minitab.com/blog/adventures-in-statistics/multiple-regession-analysis-

use-adjusted-r-squared-and-predicted-r-squared-to-include-the-correct-number-of-variables

[32] David A. Freedman, What is Error Term in a Regression Equation? Berkeley University lecture notes.

[33] Stresstech Group, MicroScan (11.7.2016). Retrieved from: http://www.stresstech.com/en-fi/products/barkhausen-noise-equipment/software/microscan/

[34] Tampere University of Techology, Suvi Santa-Aho (11.7.2016). Retrieved from: https://tutcris.tut.fi/portal/en/persons/suvi-santaaho(8204e78d-3e7f-422e-ba02-4bfc4ee45acd).html

Appendix 1

Table 1 Barkhausen noise measurements with 5 Vpp and 200 Hz magnetization parameters, magnetization in axial direction

Sample	RMS avg [mV]	RMS - [mV]	RMS + [mV]	Peak avg [mV]	Peak - [mV]	Peak + [mV]	Peak pos avg [ms]	Peak pos [ms]-	Peak pos + [ms]	FWHM avg [ms]	FWHM - [ms]	FWHM + [ms]	Coercitivity [kA/m]	Remanence [T]	Permeability [μ]	Integral area [mVs]	Spectrum area [mVs]
SG3	87.37	86.03	88.73	177.20	176.73	177.60	12.80	13.60	11.97	26.97	28.47	25.47	0.15	255.47	1693.33	248.60	13636.67
SG4	96.57	96.93	96.17	193.93	192.93	194.93	12.70	13.17	12.20	25.53	26.27	24.83	0.14	286.87	1913.67	281.40	15083.33
SG6	110.57	111.57	109.50	226.80	228.97	224.60	11.87	11.90	11.87	23.47	22.67	24.23	0.14	332.13	2342.33	312.07	17143.33
SG8	106.43	106.97	105.97	214.67	215.23	214.10	13.53	13.67	13.33	25.53	25.40	25.73	0.15	329.90	2093.33	319.23	16640.00
SG9	93.77	93.50	94.00	190.97	189.67	192.30	14.03	14.00	14.03	26.20	25.13	27.23	0.16	292.67	1898.67	285.60	14653.33
SG11	67.93	68.03	67.83	135.73	136.83	134.67	13.63	13.90	13.33	25.63	27.03	24.20	0.15	203.87	1370.67	201.60	10613.33
SG12	52.13	52.43	51.87	103.33	103.63	103.00	13.33	13.63	13.10	27.73	27.73	27.80	0.15	152.00	1040.00	153.57	8166.67
SG13	63.43	63.83	63.03	128.43	128.90	127.97	15.47	15.67	15.27	29.57	29.93	29.17	0.17	198.17	1277.67	198.97	9932.67
SG15	81.70	82.30	81.10	161.63	165.60	157.63	12.67	12.80	12.53	26.47	26.03	26.90	0.15	251.70	1718.00	240.83	12690.00
SG17	70.50	71.23	69.73	143.33	145.97	140.67	12.83	12.83	12.83	25.90	25.23	26.50	0.14	207.80	1457.00	197.07	10960.00
SG18	60.57	60.57	60.63	119.93	120.93	118.93	15.00	15.47	14.50	28.40	28.80	27.97	0.17	188.83	1214.33	193.07	9470.33
SG19	71.47	72.80	70.13	141.27	144.07	138.50	14.37	13.83	14.93	28.73	25.47	32.03	0.16	228.70	1461.67	230.77	11146.67
SG20	61.70	61.67	61.77	122.60	121.70	123.50	12.53	12.63	12.43	26.10	24.63	27.57	0.14	188.87	1286.67	179.23	9560.33
SG23	56.10	56.47	55.73	111.30	112.33	110.27	12.23	12.50	12.00	25.83	25.70	26.00	0.14	160.57	1114.33	157.20	8727.00

Table 2 XRD measurement results of sample SG03

Depth [mm]	σ [MPa]: 0.0°	(±)	σ [MPa]: 90.0°	(±)	τ [MPa]: 0.0°	(±)	τ [MPa]: 90.0°	(±)	FWHM[°]: 0.0°	(±)	FWHM[°]: 90.0°	(±)	Austenite content [%]	(±)
0	-593.6	6.7	-624.5	8.4	-78.5	1.4	-24.1	1.7	5.74	0.1	5.73	0.12	3.9	0.8
0.005	-659.8	14	-703.2	3.9	-85.5	2.9	-21.4	0.8	5.57	0.07	5.55	0.05	3.3	0.7
0.012	-754.3	4.2	-788.6	8.5	-86.7	0.9	-17.4	1.7	5.49	0.11	5.47	0.04	4.1	1.3
0.028	-946.8	5.5	-912.3	8.4	-101.7	1.1	-18.6	1.7	5.42	0.1	5.43	0.08	4.4	1.3
0.054	-1049	18.5	-1009.8	6.5	-100.8	3.8	-10.8	1.3	5.76	0.1	5.69	0.06	8.3	1.6
0.079	-969.7	11.4	-958.7	13.4	-84.5	2.3	-12.2	2.7	5.93	0.08	5.8	0.06	9	1.5
0.103	-848.2	12.7	-861.4	18.1	-57.6	2.6	-9.6	3.7	6.14	0.06	6.01	0.05	10.9	1.6
0.154	-517.3	15.2	-498.6	15.4	-42.7	3.1	-10.7	3.2	6.61	0.05	6.56	0.07	13.8	2
0.204	-360.1	19.9	-334	14.7	-25.3	4.1	-14.6	3	6.83	0.05	6.75	0.07	15.3	1.9
0.247	-265.1	25.3	-208.6	15.5	-16.1	5.2	-1.9	3.2	6.89	0.05	6.88	0.05	14.9	1.8
0.272	-221.1	14	-171.9	10.5	-11.2	2.9	-2.5	2.2	6.84	0.03	6.86	0.04	14.4	1.6

Table 3 XRD measurement results of sample SG04

Depth [mm]	σ [MPa]: 0.0°	(±)	σ [MPa]: 90.0°	(±)	τ [MPa]: 0.0°	(±)	τ [MPa]: 90.0°	(±)	FWHM[°]: 0.0°	(±)	FWHM[°]: 90.0°	(±)	Austenite content [%]	(±)
0	-529.3	10.9	-566.3	6.5	-72.9	2.2	-14.7	1.3	5.97	0.16	5.97	0.11	5.9	1.3
0.005	-730.6	8.6	-751.8	6.5	-98.1	1.8	-14.4	1.3	5.57	0.12	5.55	0.08	3.5	1
0.011	-916.6	7.5	-929.9	8.1	-125.7	1.5	-27.4	1.7	5.48	0.1	5.47	0.06	4.1	1.4
0.028	-1022.1	6.1	-1015	8.7	-117.5	1.3	-14.3	1.8	5.43	0.07	5.43	0.05	5.2	1.2
0.054	-1110.6	9.5	-1081.9	5	-103.8	2	-14.7	1	5.56	0.05	5.55	0.05	6.3	1.3
0.08	-1055.3	15.7	-1041.9	10.2	-103.2	3.2	-22.1	2.1	5.76	0.08	5.76	0.04	7.6	1.4
0.104	-949.8	20.5	-926	18.1	-78.3	4.2	-5.5	3.7	6.09	0.08	6	0.05	8.7	1.6
0.149	-606.4	17.4	-646.1	19.7	-37	3.6	11.1	4	6.53	0.06	6.46	0.08	10.7	1.7
0.2	-434.1	14	-483.4	16.9	-14.7	2.9	16.5	3.5	6.73	0.07	6.67	0.07	12.8	1.7
0.253	-352.1	19.5	-307.3	10.7	-6.4	4	10.7	2.2	6.9	0.05	6.81	0.04	13.6	1.8

Table 4 XRD measurement results of sample SG06

Depth [mm]	σ [MPa]: 0.0°	(±)	σ [MPa]: 90.0°	(±)	τ [MPa]: 0.0°	(±)	τ [MPa]: 90.0°	(±)	FWHM[°]: 0.0°	(±)	FWHM[°]: 90.0°	(±)	Austenite content [%]	(±)
0	-670.8	6.3	-662.8	7.4	46.9	1.3	-13.5	1.5	5.8	0.11	5.75	0.07	3.9	0.8
0.012	-823.9	7.8	-793.8	7.2	53	1.6	-22.3	1.5	5.57	0.07	5.61	0.06	3.8	0.8
0.026	-953.4	8.7	-898.9	5.9	48.1	1.8	-32.8	1.2	5.51	0.06	5.52	0.05	4.5	1.1
0.05	-1123.4	13.7	-1037.2	10.1	38	2.8	-35.8	2.1	5.53	0.05	5.53	0.05	5.3	0.9
0.074	-1108.3	9.9	-1029.2	8.3	10.8	2	-36.9	1.7	5.69	0.04	5.65	0.05	6.6	1.2
0.103	-962.8	21	-901.1	7.8	1.5	4.3	-33	1.6	6	0.05	5.91	0.04	8.8	1.3
0.148	-754.6	20.6	-699.8	4.5	-1.3	4.2	-26.1	0.9	6.22	0.06	6.19	0.04	10.4	1.5
0.207	-419.1	9.1	-297.5	11.5	-9.5	1.9	-15.5	2.4	6.75	0.05	6.79	0.09	12.6	0.7
0.25	-342.7	12.7	-251.6	22.9	-1.5	2.6	-10.2	4.7	6.84	0.04	6.86	0.05	12.8	1.5

Table 5 XRD measurement results of sample SG08

Depth [mm]	σ [MPa]: 0.0°	(±)	σ [MPa]: 90.0°	(±)	τ [MPa]: 0.0°	(±)	τ [MPa]: 90.0°	(±)	FWHM[°]: 0.0°	(±)	FWHM[°]: 90.0°	(±)	Austenite content [%]	(±)
0	-499.8	17.3	-552.3	17.2	-78.1	3.6	37	3.5	6.1	0.14	6.07	0.1	5.8	1.2
0.005	-586.8	9.7	-642.6	14.8	-95.4	2	45.4	3	5.77	0.14	5.71	0.06	4	0.9
0.01	-701.2	13.2	-756.5	11.9	-95.5	2.7	61	2.5	5.68	0.12	5.64	0.09	3.9	0.8
0.032	-949.3	25.9	-963.9	14.7	-124.3	5.3	80.9	3	5.61	0.08	5.62	0.03	5.2	1.1
0.06	-1067	25.3	-992.3	13.6	-86.7	5.2	70.8	2.8	5.81	0.04	5.94	0.02	7.1	1.2
0.101	-921.8	18	-734.3	12.2	-51.9	3.7	44.3	2.5	6.2	0.11	6.44	0.05	9.2	1.4
0.154	-572.7	9.9	-368.2	11.9	-10.5	2	21	2.4	6.74	0.13	6.9	0.06	11.5	1.5
0.21	-457.4	20	-326.8	15.8	-1.1	4.1	9.8	3.2	6.82	0.09	6.9	0.12	11.8	1.3
0.256	-358.2	15.7	-295.8	10.1	9.7	3.2	7.3	2.1	6.86	0.08	6.89	0.05	12.3	1

Table 6 XRD measurement results of sample SG09

Depth [mm]	σ [MPa]: 0.0°	(±)	σ [MPa]: 90.0°	(±)	τ [MPa]: 0.0°	(±)	τ [MPa]: 90.0°	(±)	FWHM[°]: 0.0°	(±)	FWHM[°]: 90.0°	(±)	Austenite content [%]	(±)
0	-535.5	10.6	-582.6	13.5	-68.1	2.2	-0.9	2.8	6.02	0.12	5.99	0.06	6	1.1
0.012	-648.2	3.7	-674	10.8	-84.5	0.8	-1.1	2.2	5.69	0.1	5.69	0.04	3.9	1.1
0.02	-690.4	5.2	-740.1	4	-87.7	1.1	-4.5	0.8	5.64	0.09	5.64	0.07	4.3	1.2
0.032	-867.6	6.7	-878.7	8.7	-103.5	1.4	1.2	1.8	5.58	0.08	5.58	0.08	4.5	1.3
0.049	-988.5	11.5	-986.5	3.5	-109.3	2.4	0.9	0.7	5.54	0.08	5.55	0.08	5.2	1.1
0.077	-1099.6	9.5	-1070.4	8.6	-94.2	1.9	7.6	1.8	5.55	0.07	5.55	0.02	6.8	1.7
0.114	-1063.9	8.8	-1041.9	11.6	-58.8	1.8	25.6	2.4	5.86	0.05	5.79	0.06	8.7	1.3
0.15	-890.9	6.7	-873	10	-35.5	1.4	17.5	2.1	6.14	0.07	6.02	0.06	10.6	1.4
0.198	-616.2	19.5	-543.5	12	-8.3	4	9.7	2.5	6.58	0.07	6.53	0.05	12.8	1.5
0.253	-426.3	19.9	-295.5	40.5	-9.8	4.1	-6.2	8.3	6.71	0.11	6.78	0.16	13.8	1.5
0.3	-408.9	17.3	-301.9	20.1	12.6	3.5	-1.5	4.1	6.77	0.09	6.78	0.07	14	1.6

Table 7 XRD measurement results of sample SG11

Depth [mm]	σ [MPa]: 0.0°	(±)	σ [MPa]: 90.0°	(±)	τ [MPa]: 0.0°	(±)	τ [MPa]: 90.0°	(±)	FWHM[°]: 0.0°	(±)	FWHM[°]: 90.0°	(±)	Austenite content [%]	(±)
0	-620.1	11.4	-602.1	4.7	-25.4	2.3	-17.9	1	6.2	0.1	6.17	0.06	7.3	1.2
0.005	-681.1	6.8	-677.2	5.2	-30.8	1.4	-19.6	1.1	5.87	0.11	5.86	0.07	6.7	1.2
0.011	-851.1	7.2	-809.2	7.8	-32.5	1.5	-15.7	1.6	5.77	0.06	5.75	0.06	6.7	1.5
0.026	-1034.1	10.9	-966.9	6.4	-26.3	2.2	-8.2	1.3	5.74	0.05	5.69	0.04	7.8	1.4
0.05	-1127.7	9.8	-1055.4	8.8	-19.7	2	-5	1.8	5.82	0.07	5.79	0.04	9.1	1.5
0.08	-1054.8	11.7	-992.7	13.1	-16.9	2.4	-0.3	2.7	6	0.05	5.97	0.07	10.5	1.6
0.101	-875.4	13.3	-833.8	7.5	-1.2	2.7	11.5	1.5	6.24	0.03	6.17	0.03	11.9	1.6
0.153	-557.7	19.9	-608.9	8.8	-24.3	4.1	17.7	1.8	6.6	0.07	6.43	0.07	13.1	2
0.212	-336.9	15.6	-286.8	22.3	-5.8	3.2	17.7	4.6	6.83	0.07	6.77	0.06	14	1.5
0.257	-314.7	18.3	-252.8	14.7	1.1	3.8	18.5	3	6.89	0.05	6.78	0.03	14.8	1.3

Table 8 XRD measurement results of sample SG12

Depth [mm]	σ [MPa]: 0.0°	(±)	σ [MPa]: 90.0°	(±)	τ [MPa]: 0.0°	(±)	τ [MPa]: 90.0°	(±)	FWHM[°]: 0.0°	(±)	FWHM[°]: 90.0°	(±)	Austenite content [%]	(±)
0	-706.4	4.9	-687.2	8.6	84.3	1	-5.3	1.8	6.36	0.08	6.37	0.07	7.7	0.7
0.005	-767.3	8.2	-759.8	12.2	66.2	1.7	-8.9	2.5	6.05	0.06	6.04	0.05	8.4	1.3
0.011	-854.3	13.5	-865.7	9.9	74.6	2.8	-15.7	2	6.01	0.06	6.01	0.04	8.3	1.1
0.054	-975.1	9.2	-909.5	9.6	56.1	1.9	-18.1	2	6.17	0.05	6.21	0.06	10.6	1.4
0.074	-859.6	12.6	-775.7	8.5	53.9	2.6	-15.4	1.8	6.4	0.07	6.39	0.03	11.7	1.5
0.103	-660.7	7.5	-646.3	14.6	43.2	1.5	-10.7	3	6.61	0.07	6.59	0.04	12.5	1.5
0.175	-324.7	23.3	-260.7	17	27.4	4.8	5.4	3.5	6.92	0.07	6.93	0.05	14.2	1.6
0.213	-277.8	14	-228.3	6.3	25.8	2.9	6.6	1.3	6.97	0.03	6.98	0.07	14.8	1.7

Table 9 XRD measurement results of sample SG13

Depth [mm]	σ [MPa]: 0.0°	(±)	σ [MPa]: 90.0°	(±)	τ [MPa]: 0.0°	(±)	τ [MPa]: 90.0°	(±)	FWHM[°]: 0.0°	(±)	FWHM[°]: 90.0°	(±)	Austenite content [%]	(±)
0	-555.6	11.4	-556.1	5.7	47.2	2.4	16.2	1.2	6.25	0.11	6.19	0.08	8.1	1
0.006	-597.8	15.8	-629.9	7	58.2	3.2	17.5	1.4	6.15	0.1	6.02	0.07	7.6	1.4
0.013	-569.7	9	-588.2	8.4	63.2	1.8	6	1.7	5.93	0.08	5.92	0.06	8.1	1.1
0.03	-839.3	13.2	-853.5	18.3	66.1	2.7	-0.1	3.8	5.83	0.06	5.82	0.07	8.1	1.4
0.048	-1003.6	8.2	-964.3	17.6	60.2	1.7	2.1	3.6	5.79	0.03	5.81	0.05	8.8	1.3
0.077	-1058.9	6.4	-984.6	15.3	54.9	1.3	2.7	3.1	5.89	0.04	5.92	0.05	10	1.3
0.104	-1004.6	7.9	-902.1	9.6	59	1.6	-2.4	2	6.02	0.06	6.11	0.06	11.1	1.3
0.15	-713.3	9.5	-642.2	13.6	60.5	1.9	5.1	2.8	6.32	0.08	6.39	0.05	12.9	1.3
0.202	-480.5	16.4	-391.8	8.2	42.7	3.4	-1.1	1.7	6.58	0.11	6.65	0.05	14.1	1.1
0.253	-354.5	16.2	-274.5	16.8	14.2	3.3	-3.9	3.5	6.78	0.07	6.79	0.04	15	1.3

Table 10 XRD measurement results of sample SG15

Depth [mm]	σ [MPa]: 0.0°	(±)	σ [MPa]: 90.0°	(±)	τ [MPa]: 0.0°	(±)	τ [MPa]: 90.0°	(±)	FWHM[°]: 0.0°	(±)	FWHM[°]: 90.0°	(±)	Austenite content [%]	(±)
0	-622.3	11.5	-618.7	8.6	-68.3	2.4	1.7	1.8	6.07	0.1	6	0.06	5.1	0.9
0.007	-657.2	7	-642.1	6.5	-75.8	1.4	0.9	1.3	5.84	0.08	5.82	0.04	4.4	1
0.015	-921.4	7.4	-836.6	9.7	-84	1.5	12.7	2	5.61	0.07	5.6	0.05	5.2	1.2
0.035	-1056.8	10.9	-964.6	9.2	-104.9	2.2	30.9	1.9	5.61	0.07	5.59	0.06	6.4	1.2
0.058	-1061.8	15.1	-1001.7	9.4	-78.3	3.1	36.3	1.9	5.91	0.08	5.75	0.04	8.1	1.5
0.088	-902	3.2	-888.6	16.6	-73.6	0.7	48	3.4	6.19	0.06	5.9	0.1	10.5	1.5
0.103	-668.1	6	-738.5	20.8	-31.7	1.2	51.3	4.3	6.58	0.04	6.21	0.09	12.3	1.6
0.164	-385.9	14.8	-328.9	10.9	-16.3	3	22.8	2.2	6.89	0.07	6.83	0.03	14.7	1.7
0.2	-342.9	12.9	-272.7	20.3	-12.8	2.6	14.1	4.2	6.94	0.09	6.9	0.03	15.3	2

Table 11 XRD measurement results of sample SG17

Depth [mm]	σ [MPa]: 0.0°	(±)	σ [MPa]: 90.0°	(±)	τ [MPa]: 0.0°	(±)	τ [MPa]: 90.0°	(±)	FWHM[°]: 0.0°	(±)	FWHM[°]: 90.0°	(±)	Austenite content [%]	(±)
0	-665.4	9.1	-668	5.9	46.6	1.9	11.4	1.2	6.07	0.07	6.04	0.07	5.2	0.8
0.006	-758.1	4.2	-776.9	3.8	56.9	0.9	-4	0.8	5.7	0.08	5.73	0.06	6.1	1
0.01	-825.2	3.5	-837.8	6.5	49.8	0.7	-2.3	1.3	5.68	0.07	5.7	0.06	5.9	1.1
0.05	-1026	9.7	-980.6	11	55.7	2	-2.5	2.3	5.71	0.03	5.71	0.05	7.1	1.3
0.076	-976.9	10.4	-934.6	10.9	47.2	2.1	-3.1	2.2	5.96	0.03	5.95	0.04	8.7	1
0.11	-840.7	16.8	-838.9	12.1	31.8	3.4	6.9	2.5	6.24	0.02	6.18	0.03	10	1.2
0.159	-519.4	14.7	-539.9	11.6	9.2	3	5.3	2.4	6.59	0.04	6.52	0.06	12	1.3
0.213	-384.7	14	-381.4	11.1	-6.7	2.9	9.3	2.3	6.68	0.06	6.72	0.05	13.1	0.9
0.26	-353.3	15.7	-306.3	22.2	4.3	3.2	4.6	4.6	6.79	0.05	6.76	0.07	13.7	1.2

Table 12 XRD measurement results of sample SG18

Depth [mm]	σ [MPa]: 0.0°	(±)	σ [MPa]: 90.0°	(±)	τ [MPa]: 0.0°	(±)	τ [MPa]: 90.0°	(±)	FWHM[°]: 0.0°	(±)	FWHM[°]: 90.0°	(±)	Austenite content [%]	(±)
0	-591.6	6.1	-575.3	8.4	-51.9	1.3	8.6	1.7	6.36	0.1	6.33	0.07	8.1	1.1
0.009	-699.3	8.1	-709	4.9	-59.5	1.7	19.1	1	6	0.07	5.95	0.07	7.6	1.5
0.015	-802.7	15.6	-829	7.1	-69.9	3.2	21.6	1.5	5.93	0.08	5.89	0.03	7.4	1.5
0.03	-883	7.4	-856.2	11.4	-69.6	1.5	24	2.3	5.95	0.08	5.92	0.06	7.5	1.3
0.07	-1039.2	9.3	-998.7	16.4	-56.8	1.9	35.2	3.4	6.19	0.05	6.16	0.04	10.6	1.6
0.101	-950.1	10.6	-896.4	14.9	-49.4	2.2	35.1	3.1	6.34	0.06	6.35	0.03	11.2	1.6
0.15	-576.1	9.9	-540.4	7.8	-22.6	2	25.5	1.6	6.71	0.07	6.67	0.04	13.8	1.7
0.202	-338.6	14	-294.6	23.2	-8.5	2.9	20.3	4.8	6.96	0.05	6.95	0.05	14.6	1.4
0.252	-234.4	20.3	-196.7	18.7	-7.2	4.2	14.2	3.8	6.99	0.06	6.91	0.04	14.7	1.6

Table 13 XRD measurement results of sample SG19

Depth [mm]	σ [MPa]: 0.0°	(±)	σ [MPa]: 90.0°	(±)	τ [MPa]: 0.0°	(±)	τ [MPa]: 90.0°	(±)	FWHM[°]: 0.0°	(±)	FWHM[°]: 90.0°	(±)	Austenite content [%]	(±)
0	-535.4	9.6	-571.8	6.3	-28.8	2	-14.5	1.3	6.1	0.14	6.02	0.08	7.6	1.2
0.006	-599.7	4.1	-632.7	9.6	-40.1	0.8	-20.4	2	5.79	0.12	5.73	0.07	4.8	0.8
0.013	-656.5	7.2	-695.1	11.4	-37	1.5	-18.8	2.3	5.7	0.06	5.67	0.07	4.5	1.1
0.036	-960.8	9.2	-931.2	14.8	-29.4	1.9	-14.6	3	5.55	0.08	5.53	0.07	5	1.1
0.051	-1037.4	14	-992.6	7.3	-27.5	2.9	-11.8	1.5	5.52	0.09	5.5	0.03	6.5	0.9
0.115	-975	17	-975.1	15.6	11.1	3.5	1.1	3.2	6.04	0.08	5.96	0.07	10.9	1.1
0.16	-509	28.9	-522.6	22.8	26.6	5.9	11.6	4.7	6.59	0.03	6.53	0.04	14.5	1.1
0.225	-378.1	18.3	-366.7	15.9	5.7	3.8	18.1	3.3	6.81	0.07	6.69	0.05	15	1.5

Table 14 XRD measurement results of sample SG20

Depth [mm]	σ [MPa]: 0.0°	(±)	σ [MPa]: 90.0°	(±)	τ [MPa]: 0.0°	(±)	τ [MPa]: 90.0°	(±)	FWHM[°]: 0.0°	(±)	FWHM[°]: 90.0°	(±)	Austenite content [%]	(±)
0	-691.2	5.4	-649.8	6.6	8.9	1.1	-16.4	1.3	6.21	0.1	6.16	0.06	6.6	0.9
0.014	-881.7	9.6	-894.3	8.3	22.5	2	-31.6	1.7	5.85	0.09	5.85	0.06	7.4	1.4
0.027	-1070	14	-1034.4	10.3	13.8	2.9	-35.1	2.1	5.85	0.05	5.87	0.05	7.8	1.5
0.051	-1026.7	6.3	-997.5	16.8	2.8	1.3	-37.6	3.5	6.01	0.06	6.09	0.06	8.5	1.4
0.072	-886	13.1	-808.8	25.4	10.1	2.7	-28.9	5.2	6.28	0.09	6.34	0.04	9.9	1.3
0.097	-675.2	23.2	-586	27.9	6.4	4.8	-18.4	5.7	6.58	0.1	6.56	0.05	12.2	1.3
0.155	-420.5	25.1	-328.2	23.3	11.3	5.2	-15.1	4.8	6.78	0.05	6.84	0.04	14	1.6
0.23	-301.5	10.2	-182.4	16.4	9.1	2.1	1.5	3.4	6.96	0.08	6.94	0.05	15.4	1.1

Table 15 XRD measurement results of sample SG23

Depth [mm]	σ [MPa]: 0.0°	(±)	σ [MPa]: 90.0°	(±)	τ [MPa]: 0.0°	(±)	τ [MPa]: 90.0°	(±)	FWHM[°]: 0.0°	(±)	FWHM[°]: 90.0°	(±)	Austenite content [%]	(±)
0	-787.9	6.7	-761.3	4.2	-63.9	1.4	-31.8	0.9	6.26	0.08	6.24	0.09	5.6	0.8
0.005	-814	11.1	-826.4	12.5	-76.4	2.3	-19.9	2.6	5.96	0.04	5.93	0.05	7.8	1.5
0.01	-851.4	9.7	-867.2	12.2	-74	2	-16.2	2.5	5.95	0.04	5.97	0.08	8.2	1.6
0.026	-938.7	4.9	-930.2	6.3	-85	1	-9.7	1.3	5.98	0.07	5.97	0.03	8.5	1.5
0.054	-965.5	18.4	-891.6	6.1	-86.1	3.8	-9.8	1.3	6.16	0.04	6.14	0.05	9.8	1.7
0.075	-879.5	13.5	-824.1	15.5	-86.2	2.8	-4.2	3.2	6.29	0.06	6.27	0.06	10.4	1.6
0.1	-659.5	15.7	-649.2	15.4	-44.3	3.2	0.6	3.2	6.54	0.04	6.47	0.05	11.6	1.8
0.149	-458.3	14.8	-496.2	8	-40.6	3	5.5	1.6	6.78	0.08	6.7	0.08	13.2	1.9
0.205	-332.8	23.3	-322.5	21.6	-25.2	4.8	8.7	4.4	6.89	0.06	6.9	0.07	13.8	1.6